

Separating Planck Bolometers and Beams via Simulated Planet Observations

Kasey W. Schultz¹

Mentors: Brendan Crill and Sunil Golwala

SURF Final Report : September 23, 2011

¹Email: k.schultz2@umiami.edu

Abstract For any Cosmic Microwave Background (CMB) observation, in order to extract the full cosmological information, the telescope beam must be accurately modeled, and the data must be corrected for the beams filtering. The CMB satellite Planck scans the full sky by rotating on its spin axis at a constant rate. This causes a degeneracy between the detector time response and the beam, and necessitates detailed modeling to identify relationships between their respective parameters. This modeling allows their effects to be separated, and produces data that has been properly corrected. Utilizing and updating the Planck teams in-place software pipeline, I have run planet observation simulations and detector and beam model reconstruction. Through identifying possible bias in the fitting routines and any degeneracy between parameters, my work provides results that will help separate these effects as much as possible. By analyzing best fit parameters of over 10,000 simulations and fits, I have shown that the pipeline reconstructs the input parameters without bias, that a variety of scenarios and phenomena produce no bias in the best fit parameters, and most importantly that prior knowledge of the beam does not bias the fitting routines or parameters; a significant result for analyzing real Planck data.

1 Introduction

Planck is a satellite-borne cosmology experiment designed to map the Cosmic Microwave Background (CMB) across the full sky. Planck's cryogenically cooled detectors are currently observing the faint glow of the Big Bang: the CMB. Planck will study the minute differences in the temperature of this radiation with respect to location on the sky, called temperature anisotropies. By studying these anisotropies, we can gain valuable insight into the origin of all large scale structure in the universe, such as galaxies and galaxy clusters. Furthermore these anisotropies can reveal the relative amounts of dark matter, dark energy, and normal matter in the universe.

The current standard cosmological paradigm includes a brief period of exponential expansion in the very early universe: inflation. Inflation solves many problems identified with the canonical Big Bang theory, but has yet to be put to the test via experiments like Planck. Even fainter than the temperature anisotropies, the polarization patterns in the CMB can reveal the details of inflation and the physics governing the universe when it was less than 10^{-30} seconds old. These polarization patterns (namely B-mode polarization) have escaped detection over the past few decades due to previous CMB satellites' low sensitivity and a lack of detailed knowledge of polarized foreground emission. By studying these anisotropies with unprecedented sensitivity and angular resolution, Planck aims to find evidence for, among many other things, primordial gravitational waves predicted by inflation by measuring the B-mode polarization signal in the CMB. If found, these primordial fluctuations would not only provide a causal explanation for the anisotropies in the CMB but also give us a window into ultra-high energy physics governing the universe at energies over a trillion times higher than those attained in particle accelerators on Earth.

Planck's predecessor, the Wilkinson Microwave Anisotropy Probe (WMAP), has already yielded important evidence supporting inflationary cosmology. Planck's higher precision on small scales is visible in the main data product that Planck, and any other CMB mission, seeks to produce, the CMB's angular power

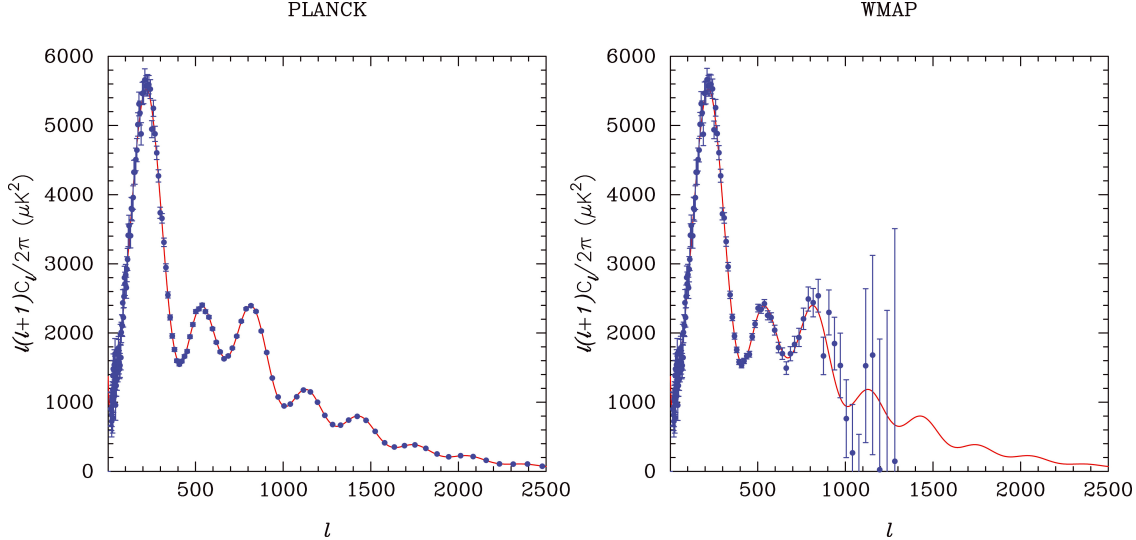


Figure 1: CMB temperature angular power spectra. Note that Planck’s increased sensitivity and resolution compared to WMAP allows for better measurement of small scale features (right side of horizontal axis). Figure adapted from The Planck Collaboration [2006].

spectra. Figure 1 shows the temperature power spectrum computed from WMAP data, and the simulated power spectrum from Planck. The vertical axis of the temperature power spectra in Figure 1 measures how different patches on the sky fluctuate up or down together in temperature (the temperature auto-correlation), while the horizontal axis is a measure of the angular size of the patches but with large scales on the left (small ℓ) and small scales (large ℓ) on the right.

2 Optical Beams and Detector Time Response

With the increasing sensitivity and resolution of Planck’s instruments, detailed knowledge of how the instrument filters the CMB signal is needed [Huffenberger et al., 2010]. My project focuses on two major contributors to overall signal distortion. First, the telescope’s beam filters the input signal, then the temperature sensitive bolometers have a finite time response to any input signal and hence further filter the data.

2.1 What is a telescope’s beam?

An optical beam is a mathematical model of the angular resolution of a telescope, that precisely describes the amount of smearing, or spatial filtering, that is done to the original input signal. In order to get the full cosmological information out of any CMB observation, the telescope beam must be accurately modeled in order to correct this spatial data filtering. Any error in beam modeling leads to error in results derived from

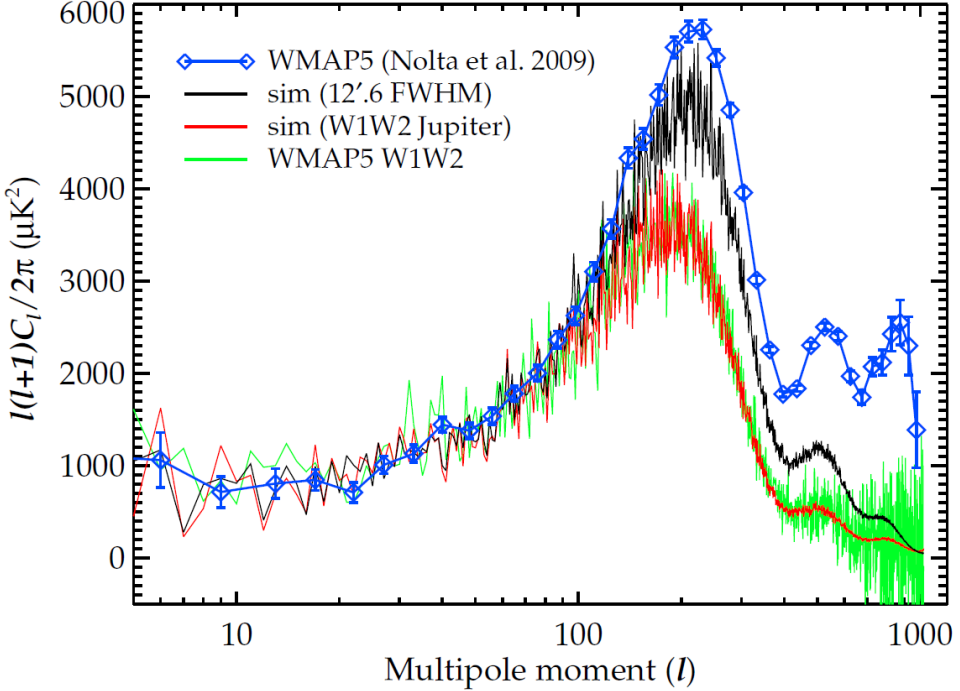


Figure 2: The temperature angular power spectrum computed from WMAP data using different beams. Note that the size and position of the first peak is affected by the different beam shapes. Figure adapted from Sawangwit and Shanks [2010].

the instrument’s data. If the beam is modeled incorrectly, then the smearing has been corrected improperly, leaving data that is not representative of the true CMB signal.

Figure 2 demonstrates that accurate beam modeling has a substantial impact on the cosmological interpretation of CMB data. In a recent paper [Sawangwit and Shanks, 2010] the authors demonstrate how different beam models impact the temperature angular power spectrum computed from WMAP data (recall Figure 1). The spectra generated from the different beams show a noticeable shift in the first peak of the spectrum. The size and position of this peak relative to the other smaller peaks reveal characteristics of the universe’s composition as a whole, and provide evidence for the existence of dark matter and dark energy. Therefore any errors in the beam correspond to errors in our understanding of the cosmos.

2.2 Beam errors can affect the entire field

Errors in Planck’s beam modeling can have negative impacts that reach even further than Planck’s own astrophysical results. These errors, if not corrected, would result in incorrect constraints by Planck on cosmological parameters. When future CMB missions are forecasting their predicted performance in terms of cosmological information gained, they will use these constraints from Planck to estimate what progress

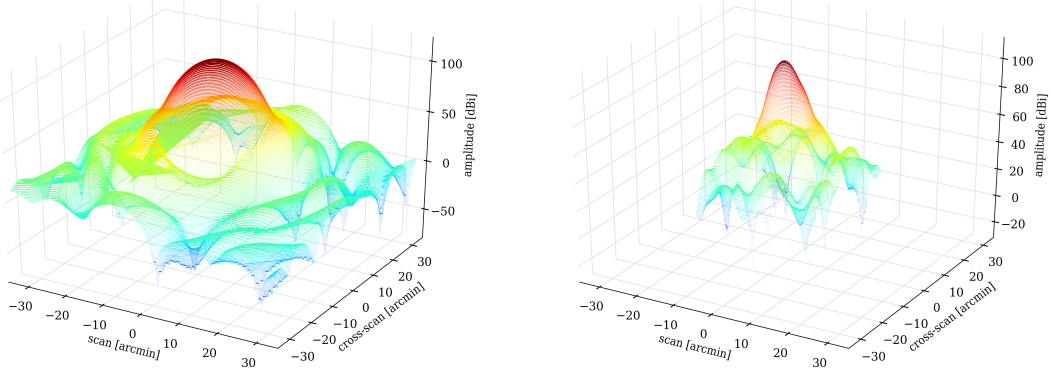


Figure 3: GRASP modeled Planck HFI beams for 100GHz (left) and 217GHz (right). The x and y axes show the beam radius in the scan and cross-scan direction in arc minutes, the z axis shows the beam amplitude in decibels relative to the beam peak. **Note:** The beam amplitude is given in dBi and hence deceptively exaggerates the beam's asymmetric side-lobes. In actuality the beam is well approximated by a best fit elliptical Gaussian function for the 100GHz and 217GHz channels.

can be made. Therefore errors with Planck can even send the entire observational cosmology community in the wrong direction with future missions.

2.3 What is bolometer time response?

In addition to the telescope's beam, the time response of the detectors can further filter the data. The Planck satellite rotates on its own spin axis, scanning the sky in great circles while it is in orbit around the sun. This combined rotation covers the entire sky in a little over seven months. Even though Planck constantly scans the sky, the photons are not detected by the bolometers and recorded instantaneously. There is actually a non-trivial time lag, or temporal filtering, while the detectors heat up due to incoming photons then transfer the energy to the heat sink and record the incident, shown in Figure 4.

2.4 Is it possible to separate their effects?

Hanany et al. [1998] show that Planck's constant scan rate leads to a degeneracy between the detector time response and the optical beam. This relationship between the two effects makes it important to separate the two effects as much as possible for analysis. The standard method of CMB data analysis has been to separate time domain effects, like detector time response, from spatial domain effects, like the optical beam. Typically the time ordered data stream is corrected for the modeled time response at the beginning of the analysis, while the beam is used at the end of the analysis when the final angular power spectra are corrected by the beam window function, which is constructed from the modeled beam. Any over or under correction for either component leads to over or under corrected data, which produces different cosmological parameters

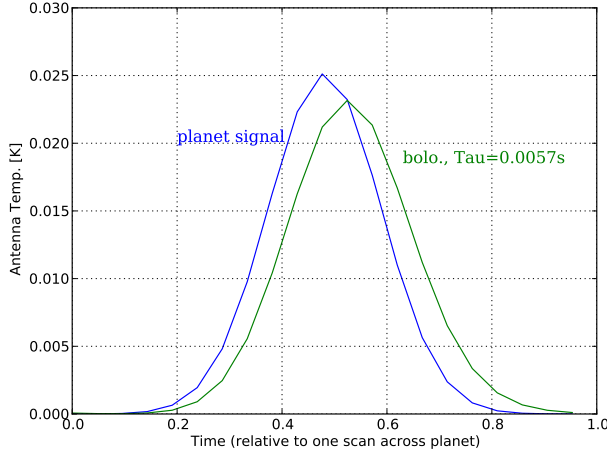


Figure 4: Simulated time-ordered signal data for a single scan across Mars. The detectors have been modeled with a single pole low-pass filter with a time constant $\tau = 5.7$ ms.

and interpretation.

3 Simulating planet observations

Historically, telescope beams have been estimated by detailed modeling of the optical systems of the telescope, by observing planets, or using both. In my analysis, I have used the GRASP modeled beams as the detailed optical system models, and have simulated planet observations. Measuring beams with planets directly follows from their resemblance to δ -functions in temperature signal. The planets are slightly smoothed from their true, point-like appearance in the sky and the shape of the smearing is an estimate of the telescope's beam.

The goal of my SURF project was to update the Planck team's in-place simulation pipeline, to include new developments in detector modeling, to simulate planet observations by Planck and to recover the best-fit optical beam parameters and time response parameters from the given beam and detector models, to interpret the fitting results and to determine how well separated the two effects are.

3.1 Basis for beam modeling

For my project, I am utilizing codes already developed by the Planck team, essentially picking up where Huffenberger et al. [2010] left off. In this paper the authors present a parametric beam model based on an elliptical Gaussian function with linear distortions in the parameters for fitting, noting that this is a simplified best-case scenario for the beam; i.e. the true beam may very well have asymmetries and extended structures referred to as "side-lobes". They also present a non-parametric basis for the beam model that

makes no assumptions of the optical systems and only relies on the planet observation data. This method provides a detailed check on the first method by only relying on the observation data, while also providing a means to characterize any asymmetries or distortions found once Planck is in orbit. This non-parametric model utilizes elliptical Hermite-Gauss basis functions. These functions reproduce an elliptical Gaussian function resembling the parametric model with the first basis coefficient, and the higher order coefficients are corrections to the elliptical Gaussian beam.

For the scope of my work, it was sufficient to compute the coefficients for these parametric and non-parametric models from a more precise model of Planck's beams based on detailed modeling of the optical systems. These models, shown in Figure 3, are obtained from the GRASP modeling software. This method produces very precise beam models from the specifics of the telescopes optical systems, however these models are not as readily incorporated into CMB data analysis as a simpler, parametrized elliptical Gaussian beam would be. This is the motivation for fitting an elliptical Gaussian beam to the data from simulated planet observations. And an important aspect of my project is to test if this assumption is an over-simplification, and if it could bias the fitting procedure in any way.

3.2 Basis for detector modeling

For the detector time response, Huffenberger et al. [2010] use a simplified single pole low-pass filter with a single time constant parameter to be fitted. However, the Planck team has recently published a paper describing a more accurate detector time response model called JH10 [Planck HFI Core Team et al., 2011]. This JH10 model is an empirical detector model that comes from lab measurements of the response of Planck's electronics.

In the JH10 model, the time response is described as the product of 3 factors H_{bolo} , H_{res} , and H_{filter} as:

$$H_{10}(f) = H_{bolo} \times H_{res} \times H_{filter} \quad (1)$$

Where H_{bolo} describes heat propagation within the bolometers as:

$$H_{bolo} = \sum_{i=1}^3 \frac{a_i}{1 + j2\pi f \tau_i} \quad (2)$$

Hence H_{bolo} has a total of 6 parameters: $a_1, a_2, a_3, \tau_1, \tau_2, \tau_3$.

And H_{res} describes the resonance of the bolometers as:

$$H_{res} = \frac{1 + p_7(2\pi f)^2}{1 - p_8(2\pi f)^2 + jp_9(2\pi f)} \quad (3)$$

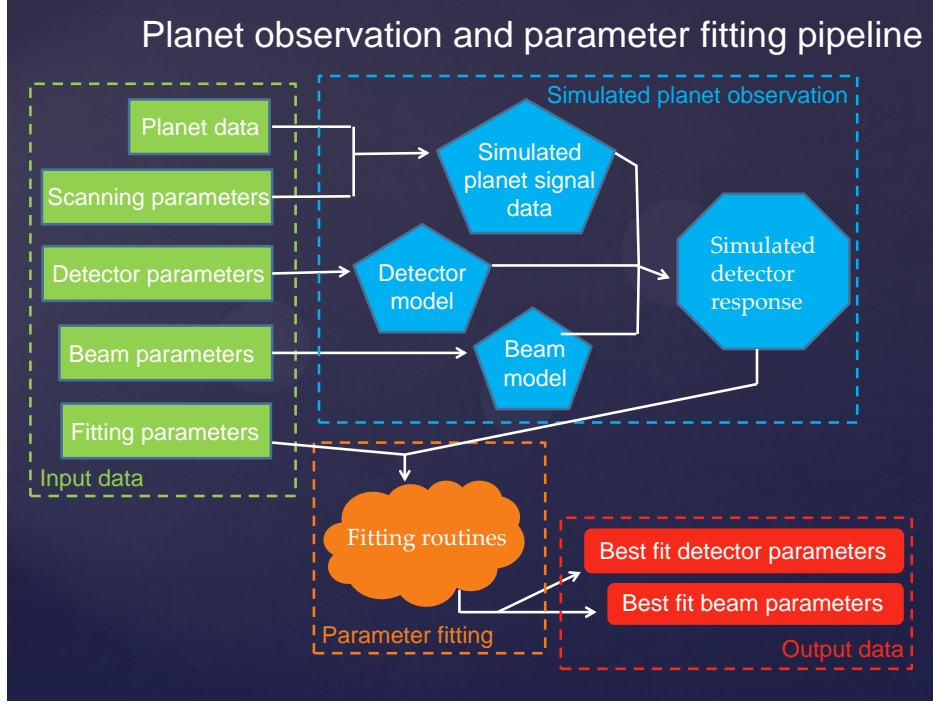


Figure 5: Basic diagram of the Planck software pipeline. Input values are in green, intermediate data products are in blue, and the final data products are in red.

Therefore H_{res} contributes an additional 3 parameters to the JH10 model: p_7, p_8, p_9 .

Finally H_{filter} describes the filtering that goes on within the bolometers themselves as:

$$H_{filter} = \frac{1 - (f/F_{mod})^2}{1 - p_{10}(2\pi f)^2 + j(f/F_{filter})^2} \quad (4)$$

So H_{filter} contributes the final parameter (p_{10}) for a total of 10 free parameters. F_{mod} and F_{filter} are kept fixed during the simulation and fitting.

3.3 Planck Simulation and Fitting Pipeline

The main goal of my project is to simulate planet observations by Planck using the JH10 bolometer response model along with the parametric and non-parametric beam models to separate the effect that these two components of the telescope have on filtering signal input. Figure 5 shows a basic diagram of the pipeline.

Simulation To simulate the signal from a planet, the pipeline gathers the ephemeris data for the specified planet; which was Mars in my analysis. The pipeline computes the planet's location, orientation and motion relative to the Planck satellite during the scan, and also computes various aspects of the planet such as its apparent disc area, flux, and other relevant values. The pipeline then generates a detector model from the

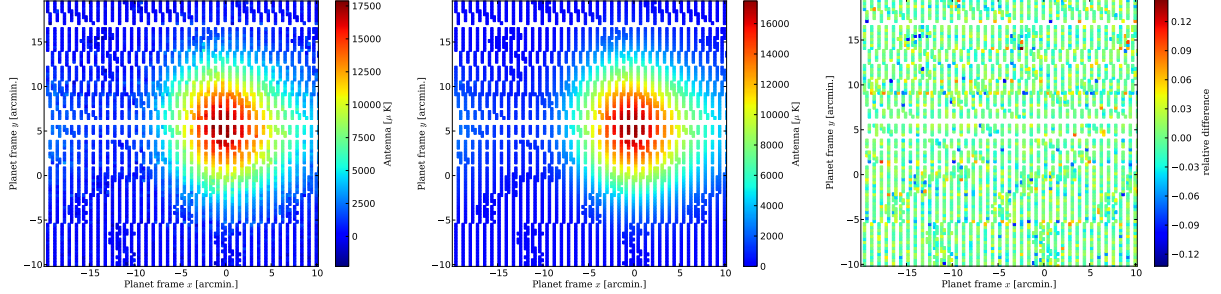


Figure 6: Left: Raw time-ordered data for detector response to simulated planet signal. Middle: Best fit model to the simulated data. Right: Residuals between signal and best fit model. **Note:** The random pointing error can be seen as deviations from parallel scans, and white space denotes areas not scanned.

JH10 parameters, and the ephemeris and other planet data is passed to the detector model. The simulated planet data and the telescope’s beam are then used to generate the detectors’ response to the input signal (Figure 6). This accurately, and quite quickly, simulates Planck’s observing the planet and the generates the data that Planck would return. For each run, there were 1024 Monte Carlo realizations of the planet observation. For each realization there were different values for detector noise, random pointing errors, fit starting values (within a neighborhood of the true input values), along with other systematic uncertainties. If we have modeled the beam and detectors correctly, in viewing the results of the simulations we should see an approximately normal distribution about the true input values, with the mean best fit parameters within about one standard deviation (1σ) of the true values (Table 1).

Fitting Once a planet observation is simulated, the pipeline moves to fitting a beam template and detector template to the detector response data. The method for optimizing the fitting parameters is described in detail in §2.6 of Huffenberger et al. [2010], but essentially the pipeline computes the best fit beam and detector parameters by minimizing the χ^2 value of the difference between the data and model; where the data is that returned from the simulated observation using the input model parameters, and the model is the new model reconstructed from the current set of fitting parameters. To minimize χ^2 as defined in equation 5, the pipeline uses a downhill simplex method, also further explained in Huffenberger et al. [2010].

$$\chi^2(\beta) = \sum_{ij} [s_i - m_i(\beta)] C_{ij}^{-1} [s_j - m_j(\beta)] \quad (5)$$

Here χ^2 is calculated for a vector, β , of the current fitting parameters by summing over the time ordered signal data s and the beam and detector model m generated from β .

3.4 Separating Beams and Bolometers

To assess how well separated beam effects are from bolometer effects, the standard method is to run simulations of planet observations given some model for the beam and some model for the detectors, then run fitting routines on the data alone to fit general beam and detector templates to the data, and finally to analyze the best fit parameters with respect to the input parameters. If the best fit parameters resemble the input models, then the fitting routines work well, but it is more important to investigate how each best fit parameter relates to the others. If you have perfectly separated the two effects, then when plotting the best fit values for each parameter against each other parameter in the run, you should see no relationships between any parameters. However, if they have not been perfectly separated, then there will be some parameters that depend on other parameters in the run. Therefore when adjusting the beam parameter, the detector parameter is inadvertently adjusted as well; this is referred to as a biased fitting routine. In the end, this results in either over or under correction for the beam's effect then the corresponding opposite under or over correction for the detectors' effects since the two are related. Your final data will then contain artificial adjustments, and hence will differ from the true CMB data.

By finding which beam and detector models that maximize data accuracy and that minimize bias in the fitting routines, one can learn a great deal about the systematics of the CMB instrument. This process leads to more accurate and physically relevant models, but more importantly it leads to a greater level of confidence and lower uncertainty in the finished data products that come from this CMB mission.

The eight separate runs described in this report (Table 1), along with the multitude of preliminary runs completed and analyzed prior to these representative final eight, aim to serve as probes on Planck's systematics and on the feasibility of using these methods to analyze true Planck data as objectively as possible.

My project probed the following sources of possible bias in the fitting routines:

- Proper motion of planet observed
- Beam size relative to scan separation
- Longer time constants in the JH10 model
- Most importantly, prior knowledge of the beam shape

Planet proper motion During the many preliminary runs that served to guide my final, and most comprehensive, eight runs, I analyzed the issue of proper planet motion. Mars does indeed move relative to Planck during observation, and it moves nearly parallel to Planck's scan direction. Mars has a proper

motion in the same direction as Planck’s scanning direction. This gives Planck better sampling in the cross-scan direction, which allows us to determine the beam parameters much more accurately than without this along-scan proper motion. This in turn can bias the resultant fitting parameters.

Beam size relative to scan separation The second item, beam size relative to scan separation, is probed by comparing runs that only differ in frequency of observation. The overall angular size of a telescope’s beam is directly proportional to the wavelength of observation, and hence inversely proportional to frequency. Therefore the higher the frequency, the smaller the angle the beam subtends on the sky (see Figure 3). Therefore when observing an object of fixed size, Mars, with different sized beams, 100GHz or 217GHz, and a fixed scan rate, the size of the beam relative to the size of the scan separation will be different. If the beam size is larger than the scan separation, then there will be an overall smoothing of the signal since there will be an overlap.

Long time constant Since the time constant parameters of the JH10 model essentially control the time response of the detectors, then it is possible that exaggerating these terms might introduce some bias. This may arise from a preference to increase some beam parameters to compensate for the increased detector filtering.

Prior knowledge of beam shape This topic is perhaps the most important of my project. In odd numbered runs, I simulate the planet observations with an elliptical Gaussian beam, and fit the same beam template to the data. However in odd numbered runs, I simulate observations with the more realistic GRASP-modeled beams, then fit an elliptical Gaussian beam model template to the data. Even though Planck’s 100GHz and 217GHz GRASP beam models differ only very slightly from these symmetric elliptical Gaussian functions, this point is crucial to test since it is most representative of true Planck data analysis. When analyzing Planck data, we can never know the true beam, however we must fit some beam template to the data in order to correct for the spatial filtering and restore the data to something more representative of the true input CMB signal. If one uses a Gaussian beam template to fit to the data and correct for filtering, then one has assumed that choosing the Gaussian beam has little to no effect on the resulting beam shape. It is indeed possible that in choosing a Gaussian beam, you are limiting the accuracy with which you restore the CMB signal.

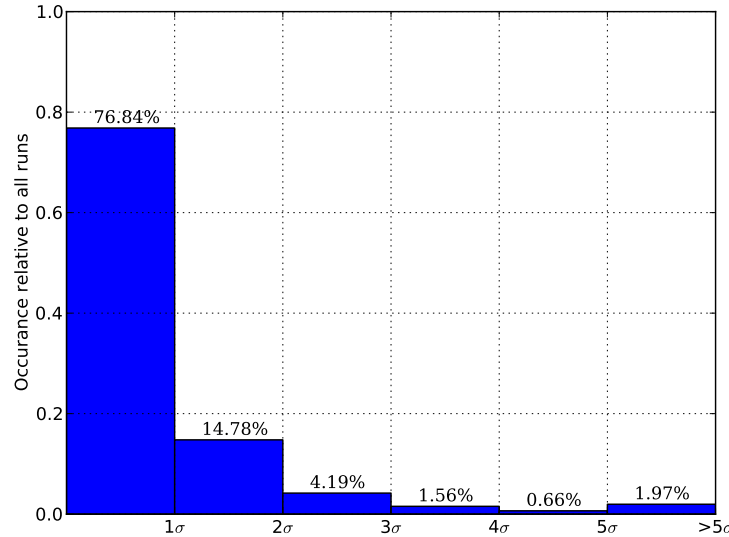


Figure 7: Distribution of all best fit parameter values compared to input values used to simulate planet observations. Note 98.03% of points are at $< 5\sigma$.

Run	#1	#2	#3	#4	#5	#6	#7	#8
Frequency	100GHz	100GHz	217GHz	217GHz	100GHz	100GHz	217GHz	217GHz
Beam model	Gaussian	realistic	Gaussian	realistic	Gaussian	realistic	Gaussian	realistic
Detect. model	JH10	JH10	JH10	JH10	JH10 long τ	JH10 long τ	JH10 long τ	JH10 long τ
beam x offset	0.0123	0.4224	0.0366	0.0356	0.0016	1.2439	0.0437	0.9001
beam y offset	0.1106	0.2350	0.0106	0.2067	0.0480	0.2291	0.0619	0.2495
gamma	0.0771	0.1442	0.1733	0.5855	0.0419	0.0265	0.1206	0.8944
mean fwhm	0.0567	1.2971	0.0590	1.5541	0.0097	1.0708	0.0282	0.2563
ellip.	0.0366	0.1444	0.0419	0.6768	0.0061	0.1205	0.0137	0.0063
a_1	0.0930	0.0038	0.1039	0.1349	0.0919	0.0995	0.1393	0.9107
a_2	0.0781	0.0269	0.1357	0.1385	0.0886	0.2047	0.1031	0.8199
a_3	0.0009	0.1902	0.0167	0.4028	0.0107	0.1205	0.0640	0.5456
τ_1	0.0124	0.4089	0.0374	0.2033	0.0752	0.8911	0.0835	0.0044
τ_2	0.0375	0.1121	0.0719	0.1608	0.0897	0.4009	0.0917	0.5070
τ_3	0.0771	0.4012	0.1098	0.5844	0.0618	0.2024	0.0047	0.6899
p_7	0.0351	0.0942	0.0016	0.0166	0.0068	0.1416	0.1032	0.0205
p_8	0.0240	0.0176	0.0542	0.9233	0.0421	0.0395	0.1076	0.2879
p_9	0.1376	0.3098	0.0147	0.4106	0.0941	0.4806	0.0487	0.3167
p_{10}	0.0075	0.3835	0.0578	0.8504	0.0522	0.4487	0.0351	0.7565
planet T	0.3504	33.3714	0.6533	1.5927	0.0873	35.1449	0.2676	3.3958

Table 1: Summarizing all 8 simulated planet observations and model fitting runs. Each run had over 1000 simulated observations (with over 10,000 time ordered data points each) and model fits. Here the values shown are $(\text{true value} - \text{mean(best fit values)}) / (\text{true value})$ expressed in terms of the parameter's standard deviation across the different best fit values in that run.

3.5 Parameter plotting pipeline

I also designed and implemented a simple software pipeline for visualizing the best fit parameters for each simulated run and investigating possible degeneracies and relationships between the fitted parameters. This pipeline reads in best fit parameter files and plots each parameter versus all the others in a matrix with each row and column corresponding to a specified parameter. This pipeline is currently implemented to plot all 16 beam and model parameters against one another in total a 120 by 120 subplot matrix. However since handling this big of a plot requires an inordinate amount of RAM (sometimes up to 16GB), the pipeline currently saves the plot in 6 separate 5 by 5 pieces.

Figures 8 and 9 were generated directly from best fit parameter data via the parameter plotting pipeline. Figure 8 shows a subset of parameter plots for a run that had most of its fits converge. The yellow and green ellipses denote the 3σ and 1σ boundaries for each parameter in the plot. a and τ_{au} are detector parameters, while the parameters on the vertical axes are for the beam model. The green stars denote the true input values for the parameters, and the plots are centered on the mean of best fit parameter values for this particular run; in Figure 8 they coincide since it is a good fit.

Figure 9 is for a run in which the majority of the fitting routines diverged. Further study of these plots can reveal degeneracies or relationships between parameters, but to avoid confusion it is best to deduce these degeneracies once the convergent and divergent fits have been separated. The parameters shown here are not the same as Figure 8, but the parameters plotted along the horizontal axes (other than planet temperature) are still for the detector model and the ones along the vertical axes are still for the beam model.

4 Conclusions

My analysis yields evidence that the following phenomena or scenarios do not bias the resulting best fit parameters in any significant way:

- Proper motion of planet observed
- Beam size relative to scan separation
- Longer time constants in the JH10 model
- Most importantly, prior knowledge of the beam shape

Proper planet motion However after analyzing similar runs with and without Mars' motion, it is clear that this has no effect on the fitting routines or on the best fit model parameters.

Beam size relative to scan separation This, as shown by comparing runs that use the same beam model and detector model and only differ by frequency, and noting that there's no difference.

Longer time constants By comparing Runs 1-4 with Runs 5-8, it seems that longer time constants do not bias the fitting routines either.

Prior knowledge of beam shape To address whether prior knowledge of beam shape introduces bias into the fitting procedures, one needs to compare odd numbered runs to even numbered runs. Odd numbered runs simulate and fit with a Gaussian beam, while even numbered runs simulate with the realistic, GRASP-modeled beam and fit with a Gaussian beam. As you can see, for even runs, there is at most one parameter out of ten per run whose mean best fit values are more than 1σ away from the true input value. There are also, for even runs, about two parameters out of ten are near 1σ from the true value. It is also very important to note that the even numbered runs have far fewer fits converge per run; about half the fits in each even numbered run reached the maximum fitting iterations before sufficiently converging. Considering these facts, my results indicate that prior knowledge of the beam shape does not introduce significant bias into the fitting routines. And this statement will be much stronger when my work is expanded to include more frequencies while taking more care to separate convergent fits from divergent fits.

5 Future Directions

My adjustments and additions to the Planck software pipeline allow expansion of this analysis to more frequencies (143GHz, 353GHz, 545GHz, 857GHz) and more planets (Jupiter, Saturn, Uranus, Neptune), with minimal change to the current state of the code. Including runs with different planets allows us to probe the affect of signal to noise ratio on the fitting routines, while including different frequencies allows us to further probe the effect of different beam sizes relative to Planck's scan separation.

Finally, by extending the pipeline to separate convergent from divergent fits within each run, it is possible to provide a more formal analysis of Planck's systematics. This would also allow the implementation of my parameter plotting pipeline to investigate which parameters have degeneracies, without being led astray by odd-looking plots from divergent fits. Comparing the statistics of convergent fits versus divergent fits will further illuminate how well the current modeling regime separates spatial filtering from temporal filtering.

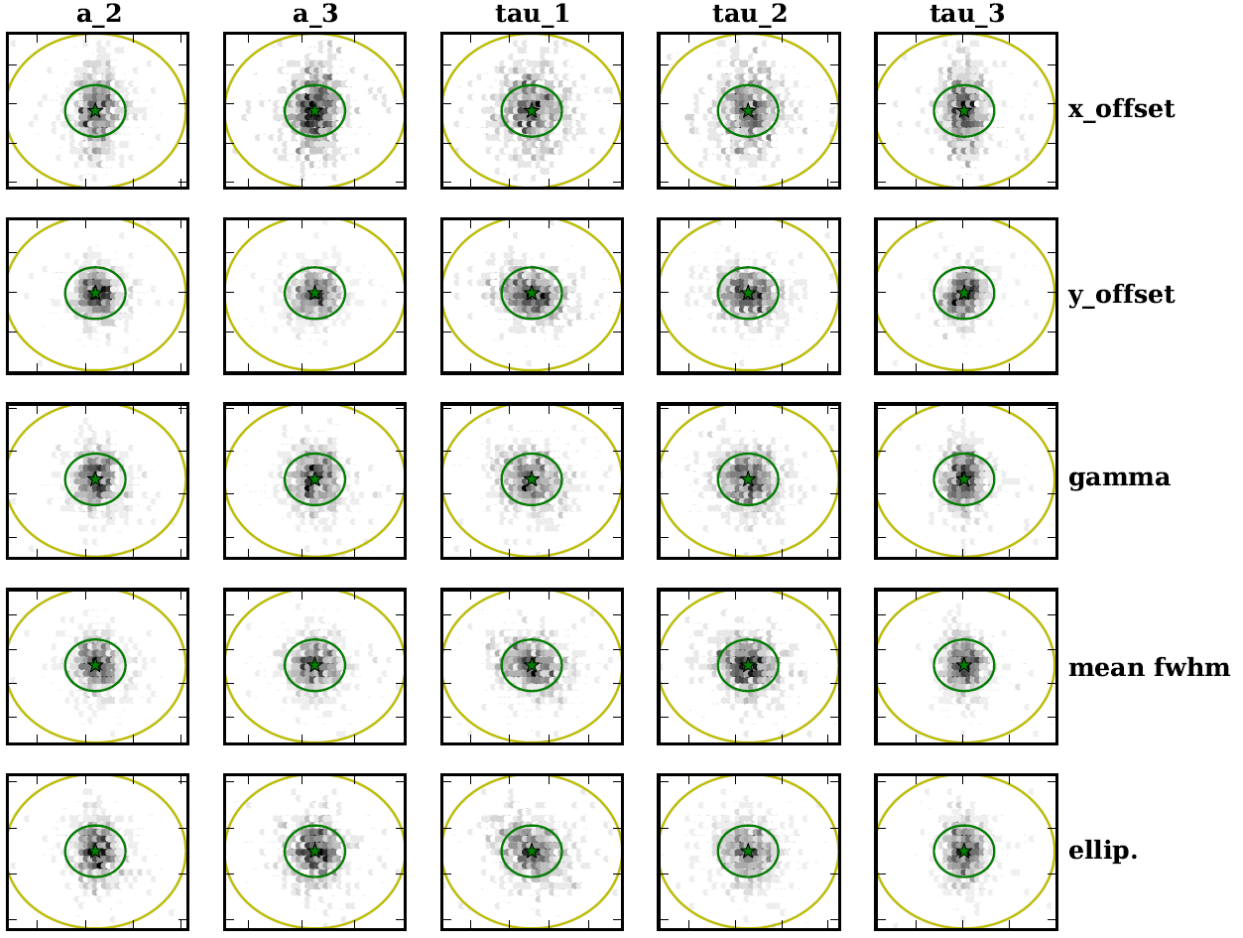


Figure 8: A subset of parameter plots from a run in which the majority of its fits converged. **Note:** Most of the best fit parameters (black dots with tone indicating density) lie mostly inside the 1σ boundary (green line) and almost all best fit values lie inside the 3σ boundary (yellow line).

Parameter	Units	Input Value	Fit Mean Value	Stnd. Dev. (σ)	Diff. Value and Mean
beam x offset	arcmin	-8.974e-01	-8.973e-01	5.261e-03	0.0123 σ
beam y offset	arcmin	1.985e-01	1.914e-01	6.468e-02	0.1106 σ
gamma	deg.	-1.448e+01	-1.455e+01	9.012e-01	0.0771 σ
mean fwhm	arcmin	9.076e+00	9.074e+00	3.778e-02	0.0567 σ
ellip.	none	1.192e+00	1.192e+00	8.380e-03	0.0366 σ
a_1	none	5.244e-01	5.288e-01	4.744e-02	0.0930 σ
a_2	none	3.369e-01	3.408e-01	5.031e-02	0.0781 σ
a_3	none	1.387e-01	1.387e-01	8.527e-03	0.0009 σ
τ_1	sec.	1.533e-02	1.534e-02	4.598e-04	0.0124 σ
τ_2	sec.	1.528e-02	1.530e-02	6.487e-04	0.0375 σ
τ_3	sec.	4.823e-02	4.863e-02	5.142e-03	0.0771 σ
p_7	none	8.486e-07	8.540e-07	1.542e-07	0.0351 σ
p_8	none	4.285e-06	4.262e-06	9.743e-07	0.0240 σ
p_9	none	2.271e-03	2.298e-03	2.004e-04	0.1376 σ
p_{10}	none	3.078e-06	3.075e-06	3.704e-07	0.0075 σ
planet T	thermo. K	2.201e+02	2.200e+02	3.366e-01	0.3504 σ

Table 2: Run 1: 100GHz, elliptical Gaussian beam, JH10

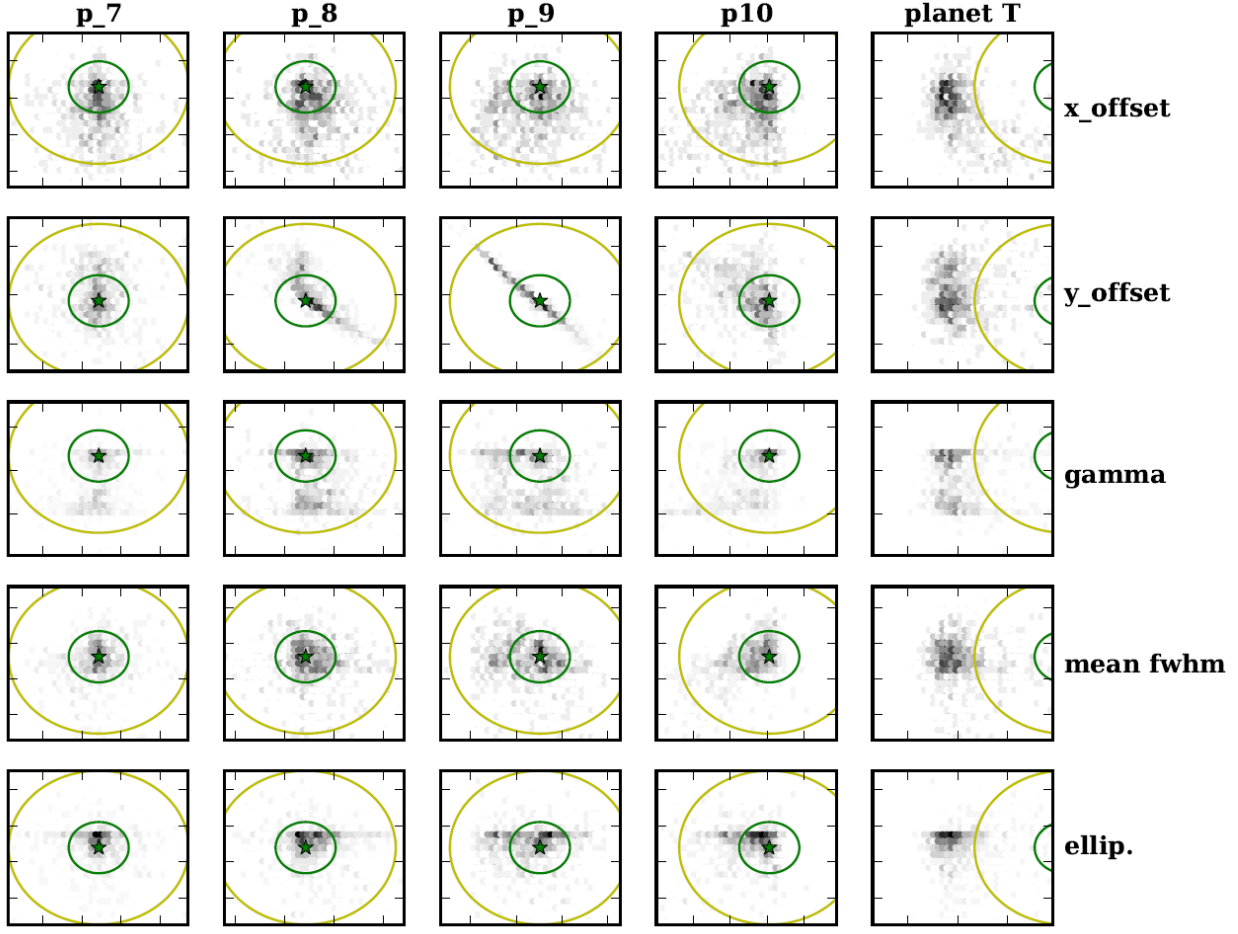


Figure 9: A subset of parameter plots from a run where most fits diverged. **Note:** Most of the best fit parameters lie outside the 1σ boundary (green line), and the mean best fit parameter values (center of the plot) do not always coincide with the true input values (star).

Parameter	Units	Input Value	Fit Mean Value	Stnd. Dev. (σ)	Diff. Value and Mean
beam x offset	arcmin	-8.974e-01	-8.997e-01	5.350e-03	0.4224 σ
beam y offset	arcmin	1.985e-01	2.369e-01	1.632e-01	0.2350 σ
gamma	deg.	-1.448e+01	-1.410e+01	2.613e+00	0.1442 σ
mean fwhm	arcmin	9.076e+00	9.191e+00	8.827e-02	1.2971 σ
ellip.	none	1.192e+00	1.195e+00	1.711e-02	0.1444 σ
a_1	none	5.244e-01	5.240e-01	1.163e-01	0.0038 σ
a_2	none	3.369e-01	3.398e-01	1.078e-01	0.0269 σ
a_3	none	1.387e-01	1.502e-01	6.043e-02	0.1902 σ
τ_1	sec.	1.533e-02	1.462e-02	1.737e-03	0.4089 σ
τ_2	sec.	1.528e-02	1.501e-02	2.365e-03	0.1121 σ
τ_3	sec.	4.823e-02	4.517e-02	7.639e-03	0.4012 σ
p_7	none	8.486e-07	8.849e-07	3.856e-07	0.0942 σ
p_8	none	4.285e-06	4.314e-06	1.616e-06	0.0176 σ
p_9	none	2.271e-03	2.434e-03	5.272e-04	0.3098 σ
p_{10}	none	3.078e-06	2.644e-06	1.132e-06	0.3835 σ
planet T	thermo. K	2.146e+02	2.258e+02	3.372e-01	33.3714 σ

Table 3: Run 2: 100GHz, GRASP beam, JH10

Parameter	Units	Input Value	Fit Mean Value	Stnd. Dev. (σ)	Diff. Value and Mean
beam x offset	arcmin	-1.018e+00	-1.018e+00	1.574e-03	0.0366 σ
beam y offset	arcmin	-9.411e-02	-9.466e-02	5.211e-02	0.0106 σ
gamma	deg.	8.003e+01	7.963e+01	2.341e+00	0.1733 σ
mean fwhm	arcmin	4.388e+00	4.386e+00	2.313e-02	0.0590 σ
ellip.	none	9.394e-01	9.397e-01	9.108e-03	0.0419 σ
a_1	none	5.244e-01	5.291e-01	4.493e-02	0.1039 σ
a_2	none	3.369e-01	3.436e-01	4.956e-02	0.1357 σ
a_3	none	1.387e-01	1.389e-01	1.051e-02	0.0167 σ
τ_1	sec.	1.533e-02	1.535e-02	4.301e-04	0.0374 σ
τ_2	sec.	1.528e-02	1.532e-02	6.433e-04	0.0719 σ
τ_3	sec.	4.823e-02	4.860e-02	3.405e-03	0.1098 σ
p_7	none	8.486e-07	8.484e-07	1.162e-07	0.0016 σ
p_8	none	4.285e-06	4.298e-06	2.260e-07	0.0542 σ
p_9	none	2.271e-03	2.273e-03	1.328e-04	0.0147 σ
p_{10}	none	3.078e-06	3.073e-06	8.474e-08	0.0578 σ
planet T	thermo. K	2.201e+02	2.200e+02	2.261e-01	0.6533 σ

Table 4: Run 3: 217GHz, elliptical Gaussian beam, JH10

Parameter	Units	Input Value	Fit Mean Value	Stnd. Dev. (σ)	Diff. Value and Mean
beam x offset	arcmin	-1.018e+00	-1.018e+00	9.982e-03	0.0356 σ
beam y offset	arcmin	-9.411e-02	-7.299e-02	1.022e-01	0.2067 σ
gamma	deg.	8.003e+01	7.277e+01	1.240e+01	0.5855 σ
mean fwhm	arcmin	4.388e+00	4.467e+00	5.113e-02	1.5541 σ
ellip.	none	9.394e-01	9.496e-01	1.508e-02	0.6768 σ
a_1	none	5.244e-01	5.469e-01	1.663e-01	0.1349 σ
a_2	none	3.369e-01	3.621e-01	1.823e-01	0.1385 σ
a_3	none	1.387e-01	1.289e-01	2.452e-02	0.4028 σ
τ_1	sec.	1.533e-02	1.549e-02	7.565e-04	0.2033 σ
τ_2	sec.	1.528e-02	1.545e-02	1.077e-03	0.1608 σ
τ_3	sec.	4.823e-02	6.387e-02	2.676e-02	0.5844 σ
p_7	none	8.486e-07	8.433e-07	3.210e-07	0.0166 σ
p_8	none	4.285e-06	4.613e-06	3.548e-07	0.9233 σ
p_9	none	2.271e-03	2.165e-03	2.581e-04	0.4106 σ
p_{10}	none	3.078e-06	2.829e-06	2.927e-07	0.8504 σ
planet T	thermo. K	2.122e+02	2.137e+02	9.310e-01	1.5927 σ

Table 5: Run 4: 217GHz, GRASP beam, JH10

Parameter	Units	Input Value	Fit Mean Value	Stnd. Dev. (σ)	Diff. Value and Mean
beam x offset	arcmin	-8.974e-01	-8.974e-01	4.936e-03	0.0016 σ
beam y offset	arcmin	1.985e-01	1.955e-01	6.277e-02	0.0480 σ
gamma	deg.	-1.448e+01	-1.452e+01	8.866e-01	0.0419 σ
mean fwhm	arcmin	9.076e+00	9.076e+00	3.848e-02	0.0097 σ
ellip.	none	1.192e+00	1.192e+00	8.295e-03	0.0061 σ
a_1	none	9.000e-01	9.047e-01	5.072e-02	0.0919 σ
a_2	none	9.000e-02	9.059e-02	6.624e-03	0.0886 σ
a_3	none	1.000e-02	1.002e-02	1.890e-03	0.0107 σ
τ_1	sec.	1.000e-02	9.987e-03	1.731e-04	0.0752 σ
τ_2	sec.	2.000e-01	2.031e-01	3.491e-02	0.0897 σ
τ_3	sec.	2.000e+00	2.018e+00	2.878e-01	0.0618 σ
p_7	none	8.486e-07	8.498e-07	1.827e-07	0.0068 σ
p_8	none	4.285e-06	4.242e-06	1.037e-06	0.0421 σ
p_9	none	2.271e-03	2.288e-03	1.817e-04	0.0941 σ
p_{10}	none	3.078e-06	3.093e-06	3.027e-07	0.0522 σ
planet T	thermo. K	2.200e+02	2.200e+02	3.314e-01	0.0873 σ

Table 6: Run 5: 100GHz, elliptical Gaussian beam, JH10 long time constant

Parameter	Units	Input Value	Fit Mean Value	Stnd. Dev. (σ)	Diff. Value and Mean
beam x offset	arcmin	-8.974e-01	-9.042e-01	5.484e-03	1.2439 σ
beam y offset	arcmin	1.985e-01	2.413e-01	1.867e-01	0.2291 σ
gamma	deg.	-1.448e+01	-1.439e+01	3.303e+00	0.0265 σ
mean fwhm	arcmin	9.076e+00	9.202e+00	1.170e-01	1.0708 σ
ellip.	none	1.192e+00	1.195e+00	2.260e-02	0.1205 σ
a_1	none	9.000e-01	8.851e-01	1.503e-01	0.0995 σ
a_2	none	9.000e-02	9.577e-02	2.821e-02	0.2047 σ
a_3	none	1.000e-02	1.052e-02	4.317e-03	0.1205 σ
τ_1	sec.	1.000e-02	9.186e-03	9.130e-04	0.8911 σ
τ_2	sec.	2.000e-01	1.717e-01	7.062e-02	0.4009 σ
τ_3	sec.	2.000e+00	2.148e+00	7.296e-01	0.2024 σ
p_7	none	8.486e-07	9.238e-07	5.312e-07	0.1416 σ
p_8	none	4.285e-06	4.208e-06	1.970e-06	0.0395 σ
p_9	none	2.271e-03	2.601e-03	6.868e-04	0.4806 σ
p_{10}	none	3.078e-06	2.453e-06	1.392e-06	0.4487 σ
planet T	thermo. K	2.140e+02	2.260e+02	3.393e-01	35.1449 σ

Table 7: Run 6: 100GHz, GRASP beam, JH10 long time constant

Parameter	Units	Input Value	Fit Mean Value	Stnd. Dev. (σ)	Diff. Value and Mean
beam x offset	arcmin	-1.018e+00	-1.018e+00	1.396e-03	0.0437 σ
beam y offset	arcmin	-9.411e-02	-9.683e-02	4.392e-02	0.0619 σ
gamma	deg.	8.003e+01	7.982e+01	1.722e+00	0.1206 σ
mean fwhm	arcmin	4.388e+00	4.387e+00	1.841e-02	0.0282 σ
ellip.	none	9.394e-01	9.395e-01	7.271e-03	0.0137 σ
a_1	none	9.000e-01	9.068e-01	4.914e-02	0.1393 σ
a_2	none	9.000e-02	9.061e-02	5.908e-03	0.1031 σ
a_3	none	1.000e-02	1.007e-02	1.028e-03	0.0640 σ
τ_1	sec.	1.000e-02	1.000e-02	5.010e-05	0.0835 σ
τ_2	sec.	2.000e-01	2.017e-01	1.880e-02	0.0917 σ
τ_3	sec.	2.000e+00	2.001e+00	1.979e-01	0.0047 σ
p_7	none	8.486e-07	8.599e-07	1.094e-07	0.1032 σ
p_8	none	4.285e-06	4.306e-06	1.907e-07	0.1076 σ
p_9	none	2.271e-03	2.276e-03	1.078e-04	0.0487 σ
p_{10}	none	3.078e-06	3.075e-06	6.456e-08	0.0351 σ
planet T	thermo. K	2.201e+02	2.200e+02	2.221e-01	0.2676 σ

Table 8: Run 7: 217GHz, elliptical Gaussian beam, JH10 long time constant

Parameter	Units	Input Value	Fit Mean Value	Stnd. Dev. (σ)	Diff. Value and Mean
beam x offset	arcmin	-1.018e+00	-1.033e+00	1.737e-02	0.9001 σ
beam y offset	arcmin	-9.411e-02	1.052e-02	4.193e-01	0.2495 σ
gamma	deg.	8.003e+01	4.820e+01	3.559e+01	0.8944 σ
mean fwhm	arcmin	4.388e+00	4.332e+00	2.179e-01	0.2563 σ
ellip.	none	9.394e-01	9.389e-01	7.102e-02	0.0063 σ
a_1	none	9.000e-01	5.435e-01	3.915e-01	0.9107 σ
a_2	none	9.000e-02	5.037e-02	4.834e-02	0.8199 σ
a_3	none	1.000e-02	1.846e-02	1.551e-02	0.5456 σ
τ_1	sec.	1.000e-02	1.000e-02	4.883e-04	0.0044 σ
τ_2	sec.	2.000e-01	4.309e-01	4.553e-01	0.5070 σ
τ_3	sec.	2.000e+00	5.600e+00	5.219e+00	0.6899 σ
p_7	none	8.486e-07	8.172e-07	1.537e-06	0.0205 σ
p_8	none	4.285e-06	4.810e-06	1.821e-06	0.2879 σ
p_9	none	2.271e-03	1.959e-03	9.854e-04	0.3167 σ
p_{10}	none	3.078e-06	2.158e-06	1.215e-06	0.7565 σ
planet T	thermo. K	2.257e+02	2.155e+02	3.007e+00	3.3958 σ

Table 9: Run 8: 217GHz, GRASP beam, JH10 long time constant

References

- S. Hanany, A. H. Jaffe, and E. Scannapieco. The effect of the detector response time on bolometric cosmic microwave background anisotropy experiments. *MNRAS*, 299:653–660, September 1998. doi: 10.1046/j.1365-8711.1998.01705.x.
- K. M. Huffenberger, B. P. Crill, A. E. Lange, K. M. Górski, and C. R. Lawrence. Measuring Planck beams with planets. *A&A*, 510:A58+, February 2010. doi: 10.1051/0004-6361/200913117.
- E. Komatsu, K. M. Smith, J. Dunkley, C. L. Bennett, B. Gold, G. Hinshaw, N. Jarosik, D. Larson, M. R. Nolta, L. Page, D. N. Spergel, M. Halpern, R. S. Hill, A. Kogut, M. Limon, S. S. Meyer, N. Odegard, G. S. Tucker, J. L. Weiland, E. Wollack, and E. L. Wright. Seven-year Wilkinson Microwave Anisotropy Probe (WMAP) Observations: Cosmological Interpretation. *ApJS*, 192:18–+, February 2011. doi: 10.1088/0067-0049/192/2/18.
- L. Page, C. Barnes, G. Hinshaw, D. N. Spergel, J. L. Weiland, E. Wollack, C. L. Bennett, M. Halpern, N. Jarosik, A. Kogut, M. Limon, S. S. Meyer, G. S. Tucker, and E. L. Wright. First-Year Wilkinson Microwave Anisotropy Probe (WMAP) Observations: Beam Profiles and Window Functions. *ApJS*, 148: 39–50, September 2003. doi: 10.1086/377223.
- Planck HFI Core Team, P. A. R. Ade, N. Aghanim, R. Ansari, M. Arnaud, M. Ashdown, J. Aumont, A. J. Banday, M. Bartelmann, J. G. Bartlett, E. Battaner, K. Benabed, A. Benot, J. . Bernard, M. Bersanelli, R. Bhatia, J. J. Bock, J. R. Bond, J. Borrill, F. R. Bouchet, F. Boulanger, T. Bradshaw, E. Brell, M. Bucher, P. Camus, J. . Cardoso, A. Catalano, A. Challinor, A. Chamballu, J. Charra, M. Charra, R. . Chary, C. Chiang, S. Church, D. L. Clements, S. Colombi, F. Couchot, A. Coulais, C. Cressiot, B. P. Crill, M. Crook, P. de Bernardis, J. Delabrouille, J. . Delouis, F. . Désert, K. Dolag, H. Dole, O. Doré, M. Douspis, G. Efstathiou, P. Eng, C. Filliard, O. Forni, P. Fosalba, J. . Fourmond, K. Ganga, M. Giard, D. Girard, Y. Giraud-Héraud, R. Gispert, K. M. Gorski, S. Gratton, M. Griffin, G. Guyot, J. Haissinski, D. Harrison, G. Helou, S. Henrot-Versillé, C. Hernandez-Monteagudo, S. R. Hildebrandt, R. Hills, E. Hivon, M. Hobson, W. A. Holmes, K. M. Huenberger, A. H. Jae, W. C. Jones, J. Kaplan, R. Kneissl, L. Knox, G. Lagache, J. . Lamarre, P. Lami, A. E. Lange, A. Lasenby, A. Lavabre, C. R. Lawrence, B. Leriche, C. Leroy, Y. L. J. F. Macas-Perez, T. Maciaszek, C. J. MacTavish, B. Maei, N. Mandolesi, R. Mann, B. Mansoux, S. Masi, T. Matsumura, P. McGehee, J. . Melin, C. Mercier, M. . Miville-Deschénes, A. Moneti, L. Montier, D. Mortlock, A. Murphy, F. Nati, C. B. Nettereld, H. U. Norgaard-Nielsen, C. North, F. Noviello, D. Novikov, S. Osborne, C. Paine, F. Pajot, G. Patanchon, T. Peacocke, T. J. Pearson, O. Perdereau, L. Perotto, F. Piacentini, M. Piat, S. Plaszczynski, E. Pointecouteau, R. Pons,

N. Ponthieu, G. Prezeau, S. Prunet, J. . Puget, W. T. Reach, C. Renault, I. Ristorcelli, G. Rocha, C. Rosset, G. Roudier, M. Rowan-Robinson, B. Rusholme, D. Santos, G. Savini, B. M. Schaefer, P. Shellard, L. Spencer, J. . Starck, P. Stassl, V. Stolyarov, R. Stompor, R. Sudiwala, R. Sunyaev, J. . Sygnet, J. A. Tauber, C. Thum, J. . Torre, F. Touze, M. Tristram, F. Van Leeuwen, L. Vibert, D. Vibert, L. A. Wade, B. D. Wandelt, S. D. M. White, H. Wiesemeyer, A. Woodcraft, V. Yurchenko, D. Yvon, and A. Zacchei. Planck early results: first assessment of the High Frequency Instrument in-flight performance. *ArXiv e-prints*, January 2011.

U. Sawangwit and T. Shanks. Beam profile sensitivity of the WMAP CMB power spectrum. *MNRAS*, pages L93+, June 2010. doi: 10.1111/j.1745-3933.2010.00894.x.

The Planck Collaboration. The Scientific Programme of Planck. *ArXiv Astrophysics e-prints*, April 2006.